Synthesis of Highly Ordered, Three-Dimensional, Macroporous Structures of Amorphous or Crystalline Inorganic Oxides, Phosphates, and Hybrid Composites

Brian T. Holland, Christopher F. Blanford, Thang Do, and Andreas Stein*

Department of Chemistry, University of Minnesota, Minneapolis, Minnesota, 55455

Received September 22, 1998. Revised Manuscript Received December 22, 1998

The synthesis of highly ordered macroporous materials has been accomplished in a straightforward, single-step reaction. Inorganic frameworks composed of oxides of Si, Ti, Zr, Al, W, Fe, Sb, and a Zr/Y mixture were formed from metal alkoxide precursors templated around polystyrene (latex) spheres. Monodisperse latex spheres were ordered into close-packed arrays by centrifugation. The interstices between latex spheres were permeated by the alkoxide, which hydrolyzed and condensed. An inorganic framework was formed upon drying. Removal of the latex spheres was accomplished by either calcination at temperatures between 450 and 1000 °C or extraction with a tetrahydrofuran/acetone mixture. The resulting products consisted of periodic, interconnected networks of monodisperse submicron pores extending over hundreds of micrometers. Depending on the technique of template removal, various phases of the inorganic oxide could be formed. For example, in the case of titania, an amorphous phase was formed upon extraction of TiO_2 and anatase by calcination at 450 °C. The synthesis has also been expanded to other compositions including aluminophosphates and hybrid organosilicates, as well as silicates with bimodal distributions of meso- and macropores. The materials presented in this paper show the diversity of macroporous materials achievable with this technique. These structures could potentially find applications as chromatographic support materials, solid catalysts, battery materials, thermal insulators, or photonic crystals.

Introduction

The discovery of the excellent sorption properties of natural zeolites in the 1940s was an incentive to develop artificial syntheses for ordered porous materials.[1] After initially mimicking geological reaction conditions, researchers began to tailor new structures by employing structure-directing agents not found in nature. Small organic molecules, for example, can help to nucleate and direct the formation of microporous structures.[2,3] One goal in structural control has been to increase the size of pores to permit penetration of larger guest molecules into the porous host structures. Until the advent of MCM-41 and related mesoporous materials, pore sizes in periodic structures were limited, with few exceptions, to a range below 2 nm.[4] In mesoporous solids, structural order and pore size control has been achieved by employing micellar arrays of surfactant molecules as structure-directing agents in a cooperative assembly process between the organic and inorganic species used. Although these materials are not crystalline like zeolites, they typically possess an ordered arrangement of pores with a narrow distribution in pore sizes. The synthesis can be tailored to produce pore sizes between 2 and 10 nm in diameter. A large assortment of mesoporous metal oxides and inorganic/organic composites has become available through modifications of the surfactant-based synthesis.[5−20] Micellar arrays have also been used to create microporous materials with

(1) van Bekkum, H.; Flanigen, E. M.; Jansen, J. C. *Introduction to Zeolite Science and Practice*; Elsevier: Amsterdam, 1991.
(2) Breck, D. W. *Zeolite Molecular Sieves*; John Wiley & Sons: New York, 1974.
(3) Derouane, E. G.; Lenos, F.; Naccache, C.; Ribeiro, E. R. *Zeolite Microporous Solids: Synthesis, Structure and Selectivity*; Kluwer Academic: 1992.
(4) Beck, J. S.; Vartuli, J. C.; Roth, W. J.; Leonowicz, M. E.; Kresge, C. T.; Schmitt, K. D.; Chu, C. T.-W.; Olson, D. H.; Sheppard, E. W.; McCullen, S. B.; Higgins, J. B.; Schlenker, J. L. *J. Am. Chem. Soc.* **1992**, *114*, 10834−10843.
(5) Huo, Q.; Margolese, D. I.; Ciesla, U.; Demuth, D. G.; Feng, P.; Gier, T. E.; Sieger, P.; Firouzi, A.; Chmelka, B. F.; Schüth, F.; Stucky, G. D. *Chem. Mater.* **1994**, *6*, 1176−1191.
(6) Corma, A.; Navarro, M. T.; Pérez-Pariente, J.; Sánchez, F. *Zeolites and Related Microporous Materials*; Weitkamp, J., Karge, H. G., Pfeifer, H., Hölderich, W., Eds.; Elsevier Science B. V.: 1994; Vol. 84, pp 69−75.
(7) Weitkamp, J.; Karge, H. G.; Pfeifer, H.; Hölderich, W. *Zeolites and Related Microporous Materials: State of the Art*; Elsevier: Amsterdam, 1994; Vol. 84.
(8) Koyano, K. A.; Tatsumi, T. *Chem. Commun.* **1996**, 145−146.
(9) Reddy, K. M.; Moudrakovski, I.; Sayari, A. *J. Chem. Soc., Chem. Commun.* **1994**, 1059−1060.
(10) Tanev, P. T.; Chibwe, M.; Pinnavaia, T. J. *Nature* **1994**, *368*, 321−323.
(11) Luca, V.; MacLachlan, D. J.; Hook, J. M.; Withers, R. *Chem. Mater.* **1995**, *7*, 2220−2223.
(12) Sayari, A.; Karra, V. R.; Reddy, J. S.; Moudrakovski, I. L. *Chem. Commun.* **1995**, 411−412.
(13) Antonelli, D. M.; Nakahira, A.; Ying, J. Y. *Inorg. Chem.* **1996**, *35*, 3126−3136.
(14) Antonelli, D. M.; Ying, J. Y. *Chem. Mater.* **1996**, *8*, 874−881.
(15) Macquarrie, D. J. *Chem. Commun.* **1996**, 1961−1962.
(16) Burkett, S. L.; Sims, S. D.; Mann, S. *Chem. Commun.* **1996**, 1367−1368.
(17) Lim, M. H.; Blanford, C. F.; Stein, A. *J. Am. Chem. Soc.* **1997**, *119*, 4090−4091.
(18) Lim, M. H.; Blanford, C. F.; Stein, A. *Chem. Mater.* **1998**, *10*, 467−470.

10.1021/cm980666g CCC: $18.00
Published on Web 02/19/1999

inorganic frameworks similar to their mesoporous counterparts.[21]

At present, several new techniques are being developed to achieve even larger mesoporous (diameters up to 50 nm) and macroporous (diameters >50 nm) solids with relatively narrow pore-size distributions. Mesopore sizes can be increased by swelling surfactant aggregates with auxiliary organic molecules,[4] by adjusting surfactant and co-cation concentrations,[22] or by postsynthesis treatment of the mesoporous sieve.[23] The condensation of a silicate network within a triblock copolymer structure and subsequent extraction of the polymer resulted in periodic mesopores with 5−30 nm diameters.[24] Macropores with diameters of a few hundred nanometers have recently been templated in inorganic solids by latex sphere dispersions in the presence of surfactants[25] and by oil/formamide emulsions.[26,27] Although these materials can have relatively narrow pore size distributions, their structural periodicity in three dimensions has been limited. Greater order has been achieved in macroporous thin silica films that were templated by surfactant-modified latex spheres deposited on a membrane as 10-μm-thick colloidal crystals.[28] We have developed a modified latex sphere templating approach that permits formation of highly ordered, three-dimensional, macroporous structures of many compositions.[29] Titania photonic crystals synthesized by a similar procedure have been shown to exhibit photonic band gaps.[30] Other related studies have described the synthesis of macroporous polyurethane membranes by a latex-sphere templating technique[31] and the preparation of periodic macroporous carbon structures by silica sphere templating.[32]

In our method, polystyrene latex spheres with a narrow size distribution are first synthesized in an emulsifier-free emulsion process. Close-packed arrays of latex spheres are formed upon centrifugation. These are dried and then placed on filter paper in a Büchner funnel. The inorganic precursors are added to the latex spheres, permeate the voids between the close-packed spheres, and condense into a hard inorganic framework upon drying. Template removal is achieved by either calcination or extraction. Depending on the choice of template removal, different phases of an inorganic material can be formed.

This paper illustrates the general applicability of this facile templating method to a variety of inorganic and hybrid macroporous structures, including oxides of Si, Ti, Zr, Al, W, Fe, Sb, and mixed Zr/Y, aluminophosphates, and organically functionalized silicates. Structural features of these materials are described, based on electron microscopy, electron diffraction (ED), powder X-ray diffraction (PXRD), adsorption methods, solid-state magic-angle spinning nuclear magnetic resonance (MAS NMR) spectroscopy, and chemical analysis. Synthetic parameters that permit control over the phase and thicknesses of the walls, as well as interconnectivity between pores, will be discussed. Many of the novel materials presented here offer distinct advantages over previously synthesized macroporous structures because of the remarkable three-dimensional periodicity of macropores, which are separated by tailorable dielectric walls. These features are requirements for new photonic crystals and can be beneficial in catalysis or large-molecule separation processes by potentially improving mass transfer processes and efficiencies. Other anticipated applications for the new macroporous solids include use as porous electrodes or electrolytes and thermal insulators.

Experimental Section

Synthesis of Surfactant-Free Polystyrene (Latex) Spheres. Non-crosslinked, monodisperse polystyrene spheres were synthesized using an emulsifier-free emulsion polymerization technique according to literature.[33] All water in the forthcoming synthetic steps was distilled and deionized to a resistivity of at least 17.6 MΩ-cm. Styrene (210 mL, Aldrich) was washed in a separatory funnel four times with 200 mL of 0.1 M NaOH (EM Science), then four times with 200 mL of water. A five-necked, 3000-mL round-bottomed flask was filled with 1700 mL of water and heated to 70 °C before 200 mL of the washed styrene was added. Attached to the flask was an electric motor driving a glass stirring rod and Teflon wedge, a thermometer, a condenser, a pipet through which house nitrogen was bubbled to deaerate the mixture, and a stopper for the addition of reactants. In a separate 160-mL polyethylene bottle, 0.663 g of potassium persulfate initiator (Fisher) was added to 100 mL of water, and the solution was then heated to 70 °C. The water and styrene solution was reheated to 70 °C, and the initiator was added. To facilitate later removal of the latex spheres from the macroporous product, no cross-linking agent was added. The temperature was kept at 70 ± 2 °C while the solution was stirred at 245 or 360 rpm for 28 h. The resulting latex spheres were filtered through glass wool to remove any large agglomerates. The latex spheres remained suspended in their mother liquor until needed. Before use, the spheres were centrifuged at 900−1000 rpm (k-factor $\approx 3.1 \times 10^5$) for 12 to 24 h, then allowed to air-dry. In the present studies, spheres with diameters ranging from 421 ± 40 nm to 697 ± 64 nm were produced at stir rates between 245 and 360 rpm, keeping all other experimental conditions the same. The diameters of the spheres were estimated using scanning electron microscopy (SEM).

Synthesis of Macroporous Solids. *Macroporous Oxides.* The alkoxide precursors employed for each macroporous solid were used as received without further purification. Tetraethoxysilane (TEOS, 98%), tetramethoxysilane (TMOS), aluminum tri-*sec*-butoxide (97%), zirconium *n*-propoxide (TPZ, 70%, in propanol), and vinyltriethoxysilane (VTES) were obtained from Aldrich; titanium(IV) ethoxide (TET, 95%), antimony(III) *n*-butoxide, iron(III) ethoxide, vanadium tri-*n*-

(19) Aronson, B. J.; Blanford, C. F.; Stein, A. *Chem. Mater.* **1997**, *9*, 2842−2851.
(20) Holland, B. T.; Isbester, P. K.; Blanford, C. F.; Munson, E. J.; Stein, A. *J. Am. Chem. Soc.* **1997**, *119*, 6796−6803.
(21) Sun, T.; Ying, J. Y. *Nature* **1997**, *389*, 704−706.
(22) Corma, A.; Kan, Q.; Navarro, M.; Pérez-Pariente, J.; Rey, F. *Chem. Mater.* **1997**, *9*, 2123−2126.
(23) Khushalani, D.; Kuperman, A.; Ozin, G. A.; Tanaka, K.; Garcés, J.; Olken, M. M.; Coombs, N. *Adv. Mater.* **1995**, *7*, 842−846.
(24) Zhao, D.; Feng, J.; Huo, Q.; Melosh, N.; Fredrickson, G. H.; Chmelka, B. F.; Stucky, G. D. *Science* **1998**, *279*, 548−552.
(25) Antonietti, M.; Berton, B.; Göltner, C.; Hentze, H. P. *Adv. Mater.* **1998**, *10*, 154−159.
(26) Imhof, A.; Pine, D. J. *Nature* **1997**, *389*, 948−951.
(27) Imhof, A.; Pine, D. J. *Adv. Mater.* **1998**, *10*, 697−700.
(28) Velev, O. D.; Jede, T. A.; Lobo, R. F.; Lenhoff, A. M. *Nature* **1997**, *389*, 447−448.
(29) Holland, B. T.; Blanford, C. F.; Stein, A. *Science* **1998**, *281*, 538−540.
(30) Wijnhoven, J. E. G. J.; Vos, W. L. *Science* **1998**, *281*, 802−804.
(31) Park, S. H.; Xia, Y. *Chem. Mater.* **1998**, *10*, 1745−1747.
(32) Zakhidov, A. A.; Baughman, R. H.; Iqbal, Z.; Cui, C.; Khayrullin, I.; Dantas, S. O.; Marti, J.; Ralchenko, V. G. *Science* **1998**, *282*, 897−901.
(33) Wang, L. Ph.D. Thesis, University of Minnesota, Minneapolis, MN, 1993.

Table 1. Weight Percent of Inorganic Solid Remaining After Template Calcination for Various Weight Ratios of Alkoxide, Alcohol, and Latex Spheres

alkoxide, alcohol[a]	alkoxide/ alcohol (wt:wt)	alkoxide/ spheres (wt:wt)	remaining inorganic after calcination[b] (wt %)
TEOS, ethanol	100:0	10.0	5.2
	70:30	7.0	2.9
	55:45	5.5	5.5
TET, ethanol	100:0	5.4	10.0
	43:57	2.7	8.9
	29:71	1.8	6.3
	14:86	1.1	2.9
	13:87	0.7	4.2
TPZ, 1-propanol, ethanol	70:30	3.0	12.7
	40:60	1.8	13.5
	21:79	1.0	5.9
	18:82	0.9	6.7
	15:85	0.7	5.0

[a] Macroporous aluminum oxide/hydroxide. In a typical sample preparation a 1.5:1 ratio of the aluminum tri-sec-butoxide/2-butanol/latex sphere composite was formed. Template removal was achieved by calcination at 575 °C in air for 7 h, leaving 10.5 wt % of the inorganic product. [b] Determined by TGA for silica samples, by weighing before and after calcination for titania and zirconia samples.

propoxide, tungsten (V) ethoxide (95%), copper(II) ethoxide, cerium(IV) isopropoxide, yttrium isopropoxide (95%), and zirconium *n*-propoxide (70%) were purchased from Gelest, and 2-cyanoethyltrimethoxysilane (CETMS) was from United Chemicals. The macroporous solids were prepared as previously described.[29] Millimeter-sized chunks of dried latex spheres were added to a Büchner funnel attached to a vacuum of ≈100 mTorr and wetted with ≈1 mL of absolute ethanol. The liquid alkoxides were then added by pipet until the spheres were completely wetted. Most liquid alkoxides could be used neat. By diluting the alkoxides in ethanol, it was possible to adjust the viscosity and hydrolysis/condensation rates of the alkoxide. Especially in the case of TET and TPZ, dilution with ethanol suppressed premature metal oxide precipitation upon exposure to air. The relationships between the alkoxide concentration in alcohol and the structure of the macroporous solids was studied for a number of concentration series listed in Table 1. In the synthesis of macroporous alumina, the high viscosity and reactivity of aluminum tri-*sec*-butoxide made it necessary to dilute it to 50 wt % with 2-butanol. Solid iron(III) ethoxide was prepared as a 25 wt % solution in ethanol. About 6 mL of solution was used per 0.25 g of dried spheres. Copper(II) ethoxide, cerium(IV) isopropoxide, and yttrium tri-isopropoxide by themselves were too insoluble in their corresponding alcohols to allow an ordered macroporous structure to form. Solid yttrium isopropoxide could be dissolved in 70 wt % zirconium *n*-propoxide in propanol to give a Zr/Y mole ratio of 22:1.

The coated latex spheres were dried in air or a vacuum desiccator for 3−24 h. Polystyrene was removed from the inorganic framework by calcination in air at 450−575 °C for 6−8 h (575 °C for oxides of Ti, Al, Si, Zr; 450 °C for oxides of Sb, W, Fe, Ge, V, Zr/Y), or at 1000 °C for 2 h to study phase changes in titania samples. Alternately, to attain milder conditions, polystyrene was extracted by Soxhlet extraction for 1−6 d in a 1:1 (v/v) mixture of tetrahydrofuran (THF) and acetone.

Aluminophosphates. First, 2.04 g of aluminum isopropoxide (Eastman), 1.15 g of 85% H_3PO_4 (Aldrich), 3.64 g of 25% tetramethylammonium hydroxide (TMAOH, Aldrich) and 2.94 g of water were mixed in a polyethylene bottle. The resultant white solution was rapidly stirred for at least 17 h before use, at which time it was added to the latex spheres. The latex spheres coated with aluminophosphate were dried overnight in air and then calcined at 850 °C in air for 7 h.

Silicates with Mesoporous Walls. An aqueous mixture containing 20 mL of 8 wt % cetyltrimethylammonium hydroxide (CTAOH), 2.1 g of TEOS, and 1.0 g of 1 M tetrapropylammonium hydroxide (TPAOH, Aldrich) was stirred at 70 °C for 1 h, filtered, and allowed to permeate through the packed polystyrene spheres. The product was dried and calcined at 575 °C in air for 6 h.

Silicates with Organic Functional Groups. Hybrid organic/inorganic sieve structures were synthesized using mixtures containing 1.8−9.1 TEOS:1.0 VTES:8.3−41 ethanol, or 5.8−17 TMOS:1.0 CETMS:27−82 methanol (mole ratios) as precursors. In a Büchner funnel, a 2−4-mm layer of dried latex spheres was placed on filter paper. Approximately 2−4 mL of the mixed precursor solution was added to the spheres. The organosilicate/latex sphere composites were dried overnight in a vacuum desiccator. The latex spheres were removed from the inorganic/organic composites by extracting for 1−6 d with a 1:1 (v/v) mixture of THF and acetone in a Soxhlet extractor.

Product Analysis. Powder XRD studies were performed on a Siemens D5005 wide-angle XRD spectrometer with Cu Kα radiation, operating at 40 kV and 45 mA. In a typical sample preparation, the template-free macroporous materials were gently crushed with a mortar and pestle and placed in low-background, off-axis quartz cells with cavities 1 mm deep and 12 or 20 mm in diameter. For particle-size determinations based on the Scherrer equation, the macroporous materials were ground together with a potassium halide (KCl, KBr, or KI) as a line width standard. Scanning electron micrographs were recorded digitally with a Gatan Digiscan and Digital Micrograph on a JEOL 840 SEM operating at 7 kV. Samples for SEM were dusted on an adhesive conductive carbon disk attached to an aluminum mount. The samples were then coated with 5 nm Pt or Au/Pd. Transmission electron micrographs (TEM) were recorded on film with a Philips CM30 TEM operating at 300 kV with a LaB_6 or W filament. Samples for TEM were prepared by sonicating ≈20 mg of the powder in 2 mL of absolute ethanol for 30 min, then depositing five drops of the suspension on a holey carbon grid. Micrographs were scanned on a Microtek ScanMaker III scanner for further analysis. A fast Fourier transform (FFT) was used to analyze the spatial periodicity of the structure. The structure was indexed by correlating the FFT pattern and TEM goniometer tilt to theoretical diffraction patterns. Energy dispersive spectra (EDS) were acquired using an EDAX PV9900 equipped with an ultrathin window Si(Li) detector. Spectra were acquired with the sample tilted 30° toward the detector for 200 s live time. Chemical analyses were carried out for C, H, and S at Atlantic Microlabs Inc., Norcross, GA, and for Si, Ti, Zr, Al, and P at the Geochemical Lab, University of Minnesota, Minneapolis, MN. Nitrogen adsorption measurements were performed on a RXM-100 sorption system (Advanced Scientific Designs, Inc.) or a Micromeritics ASAP 2000 V3.00 sorption analyzer utilizing Brunauer−Emmett−Teller (BET) calculations of surface area and Barrett−Joyner−Halenda (BJH) calculations of pore volume and pore size distributions for the adsorption portion of the isotherm. Mercury porosimetry measurements were carried out on a Micromeritics Poresizer 9320. Thermogravimetric analysis (TGA) was performed on a Perkin-Elmer TGA-7 thermal analyzer attached to a personal computer (PC) via a TAC7/DX thermal controller. The samples were heated under flowing air from 30 to 800 °C at 10 °C/min. Solid-state ^{29}Si (79.4 MHz, pulse width 4 μs, pulse delay 300 s, 254 transients, 3 kHz spin rate), ^{27}Al (104.3 MHz, pulse width 30 μs, pulse delay 1.5 s, 16 384 transients, 3 kHz spin rate), and ^{31}P (162.0 MHz, pulse width 4 μs, pulse delay 10 s, 512 transients, 3 kHz spin rate) MAS NMR measurements were performed on a Chemagnetics CMX Infinity spectrometer. Tetramethylsilane (TMS), 1 M $Al(H_2O)_6^{3+}$, and 85% H_3PO_4 were used as external chemical shift standards. Fourier transform infrared (FT-IR) spectra were collected on a Nicolet Magna FT-IR 760 spectrometer from samples prepared as KBr pellets.

Results and Discussion

Ordering the Latex Spheres. Colloidal crystals of latex spheres in two and three dimensions (2D and 3D)

are well-known.[34−40] They can be formed by slow sedimentation or by centrifugation of colloidal dispersions of spherical particles. During the formation of 2D crystals, spheres are ordered into close-packed arrays by attractive capillary forces (from the menisci formed around the spheres) and by convective transport of particles toward the ordered regions.[41,42] The crystallization of 3D colloidal arrays is controlled by repulsive electrostatic forces between spheres. It is possible to induce crystallization from a suspension of latex spheres by increasing the volume fraction of spheres in the suspension.[35] The most ordered arrays can be formed by slow sedimentation,[40] but faster ultracentrifugation can also result in the formation of periodic colloid structures.[43] Centrifugation concentrates the disperse spheres in a smaller volume, removing solvent from the space between spheres, and often leading to close-packing.[44]

Sedimentation of monodisperse latex spheres into hexagonally close-packed layers can, in principle, result in hexagonally close packed (hcp), face-centered cubic (fcc) close packed, or random stacking in the third dimension. Body-centered cubic (bcc) phases have also been observed, especially at low concentrations of spheres in a suspension, in the presence of foreign salts, or at elevated temperatures.[35,36,38] Although the free energy differences between hcp and fcc are small, recent computer simulations by Woodcock have indicated that stacking of hard spheres in an fcc arrangement is the most stable arrangement.[45] Experimentally, preferred fcc crystallization has been confirmed for crystals of monodisperse silica nanospheres (0.2−0.5 μm diameters) grown by natural sedimentation,[46] and for crystals of latex spheres (0.24 μm diameter) grown by centrifugation.[40] An fcc arrangement in a set direction has also been forced by slow sedimentation of colloidal particles onto a patterned substrate.[47]

In our study, centrifuging the latex spheres resulted in the formation of an iridescent sediment on the bottom of the centrifuge tube with a clear solution on top. The clear solution was decanted, and the latex spheres were air-dried before treatment with the network-forming solutions. To obtain periodic void structures, it was critical to employ uniformly sized templates. Scanning electron micrographs show the monodispersity of the latex spheres, Figure 1. It should be noted that the centrifuged spheres were already ordered into close-packed domains at this stage before any alkoxide had been added. Although the latex sphere arrays contained stacking faults, point defects, line defects, and larger disordered regions, Figure 1 shows facets corresponding to the {100}, {011}, and {111} sets of planes that typify an fcc structure. These observations are similar to reported findings for silica nanospheres.[46] It was difficult to determine the phase purity of the close-packed spheres by SEM because the number of spheres in a typical centrifuged sample was quite large. Phases other than fcc or disordered phases may be present. However, the fcc structure was observed in templated macroporous silica, titania, zirconia, and zirconia/yttria particles (vide infra).

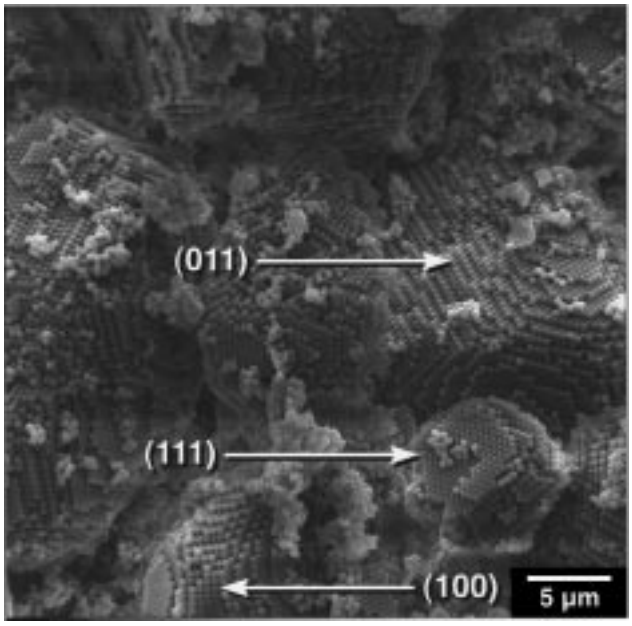

Figure 1. SEM of small colloidal crystals composed of monodisperse latex spheres. These were used as templates for the inorganic composites. Exposed (100), (111), and (011) faces are labeled.

Some disorder observed by SEM was likely created during the preparation of these brittle colloidal crystals for electron microscopy. Although large defects were templated into the inorganic product, healing of smaller defects by capillary effects was conceivable during wetting of the colloidal latex crystal. Nonetheless, it appeared that close-packing of the spheres was critical *before* alkoxide addition to result in the highest amount of ordered product *after* addition of the inorganic components and subsequent template removal. In experiments when TEOS/ethanol solutions were added to completely disordered latex spheres, ordering did not occur upon evaporation of ethanol and condensation of the silicate. Additionally, when latex films were created by evaporation instead of centrifugation, neither the polymer film nor the templated product were ordered on a micrometer scale. Methods of growing larger ordered regions of latex spheres must be employed to template large inorganic macropore structures; these techniques will be addressed in future work.

Addition of Inorganic Precursors. Percolation of alkoxides through the latex spheres produced highly ordered composite structures. In fcc or hcp structures, ≈74% of the volume is occupied by the monodisperse

(34) Ottewill, R. H. *Langmuir* **1989**, *5*, 4−11.
(35) Larsen, A. E.; Grier, D. G. *Nature* **1997**, *385*, 230−233.
(36) Okubo, T. *J. Chem. Soc., Faraday Trans.* **1990**, *86*, 2871−2876.
(37) Okubo, T.; Kiriyama, K. *Ber. Bunsen-Ges. Phys. Chem.* **1996**, *100*, 849−856.
(38) Carlson, R. J.; Asher, S. A. *Appl. Spectrosc.* **1984**, *38*, 297.
(39) Pusey, P. N.; van Megen, W.; Bartlett, P.; Ackerson, B. J.; Rarity, J. G.; Underwood, S. M. *Phys. Rev. Lett.* **1989**, *63*, 2753−2756.
(40) Vos, W. L.; Megens, M.; van Kats, C. M.; Bösecke, P. *Langmuir* **1997**, *13*, 6004−6008.
(41) Denkov, N. D.; Velev, O. D.; Kralchevsky, P. A.; Ivanov, I. B.; Yoshimura, H.; Nagayama, K. *Langmuir* **1992**, *8*, 3183−3190.
(42) Denkov, N. D.; Velev, O. D.; Kralchevsky, P. A.; Ivanov, I. B.; Yoshimura, H.; Nagayama, K. *Nature* **1993**, *361*, 26.
(43) El-Aasser, M. S.; Robertson, A. A. *J. Colloid Interface Sci.* **1971**, *93*, 504−512.
(44) Efremov, I. F. *Surface and Colloid Science*; Matijevic, E., Ed.; Wiley: New York, 1976; Vol. 8, pp 85−192.
(45) Woodcock, L. V. *Nature* **1997**, *385*, 141−143.
(46) Míguez, H.; Meseguer, F.; López, C.; Mifsud, A.; Moya, J. S.; Vázquez, L. *Langmuir* **1997**, *13*, 6009−6011.
(47) van Blaaderen, A.; Ruel, R.; Wiltzius, P. *Nature* **1997**, *385*, 321−324.

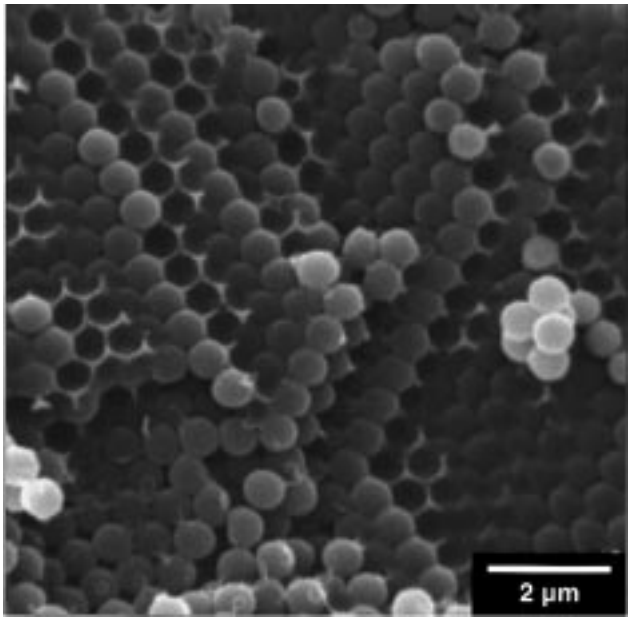

Figure 2. SEM of a latex sphere array that had been infiltrated with TEOS and dried at room temperature.

spheres; in bcc lattices, the value is ≈68%. The remaining 26 or 32% of volume can, in principle, be filled by the inorganic precursors. The liquid alkoxides might also penetrate the internal volume of the non-crosslinked latex spheres, although at present we do not have any direct evidence for this process. The SEM image in Figure 2 depicts the composite structure obtained after TEOS was added to an array of polystyrene spheres to coat the spheres. The spaces between spheres were filled by layers of partially condensed silica, indicating that the inorganic precursor was able to diffuse through the interstitial voids between the close-packed spheres during the vacuum-assisted percolation process. In addition, individual spheres were visible, as well as hollow silica replicas of spheres that probably were dislodged during sample preparation (fracturing) for SEM. From the SEM images it could not be determined whether individual spheres were coated with silica; however, in some calcined samples, isolated hollow spheres of the inorganic oxide were observed. These hollow spheres must have formed around polystyrene spheres that had become dislodged from the colloidal crystal.

It is interesting that condensation of the metal alkoxides, including TEOS, occurred upon drying of the latex/alkoxide composites in air, without the addition of an external acid or base catalyst. Initially, the composite materials were soft and pliable, but they hardened over a period of minutes (titania, zirconia) to hours (silica), depending on the reactivity of the alkoxide in air, the temperature, and the humidity. It is possible that protonated carboxyl groups present on the surface of the latex spheres[48,49] catalyzed the hydrolysis and condensation reactions. Further condensation occurred during template removal by thermal methods.

Removal of Latex Spheres. Removal of the latex spheres was typically accomplished by calcination in air at temperatures ranging from 450 to 1000 °C. As the organic template escaped, it created windows between adjacent voids. Based on the carbon content of the products (0.4 to 1.0 wt %), the organic components were nearly completely removed. The amount of inorganic solid remaining after latex sphere removal was ≈3−14 wt % of the composite material, based on TGA measurements. The maximum theoretical values, assuming complete filling of the interstitial spaces in a close-packed structure with alkoxide, were 8.0 wt % for SiO_2 from TEOS, 9.9 wt % TiO_2 from TET, and 8.2 wt % ZrO_2 from 70% zirconium *n*-propoxide. These theoretical yields are based on the combined mass of polystyrene spheres and alkoxide. Lower yields can be attributed to incomplete filling of interstitial space; higher yields imply expansion of colloidal crystal or formation of a dense phase with low porosity (vide infra).

In an alternative procedure, the polystyrene could be extracted with a THF/acetone solution. An ordered macroporous structure was maintained after extraction. However, the windows connecting the spheroidal voids were often smaller or absent after the extraction process. Nonetheless, based on IR spectroscopy, most polystyrene was removed after extraction. The conditions of template removal affected the phase of the walls in the macroporous product. Low-temperature calcination or extraction could produce macroporous structures with amorphous walls, which, in turn, exhibited micro- or mesoporosity and high surface areas. Higher temperature calcination permitted the formation of crystalline walls. Extraction was also useful to avoid high temperatures in order to preserve organic moieties.

Description of the Inorganic Replica Structure. A structural description for these solids has to cover multiple hierarchies, including the macroporous structure, and the structure within the wall at the atomic level or sometimes the mesoscopic level. These hierarchies will be discussed in more detail in this section.

Macroporous Level. The macroscopic structure of the inorganic solids was predetermined by the arrangement of the latex sphere templates. The void diameters depended on the size of the latex spheres. It should be noted that, typically, 26−34% shrinkage of the structure occurred during calcination. These results are similar to observations by other groups for macroporous[28] and mesoporous silica samples.[50] These shrinkage data were average values measured by comparing a large number of pore center-to-center distances in the template-free samples with center-to-center distances in the templating latex sphere arrays. Based on the relatively narrow pore size distributions observed by SEM and TEM, contraction appeared to occur uniformly throughout the samples. Extraction diminished the amount of shrinkage only slightly. For example, for a sample of macroporous titania, 34% shrinkage was observed upon calcination and 24% upon extraction.

Although monodispersity of the spheres was critical to obtain periodic void structures, the overall frameworks exhibited similar structures for samples prepared from spheres of different diameters between ≈420 and 700 nm. Areas exhibiting close packing of pores were seen over tens (Figure 3) and sometimes hundreds of

(48) Goodwin, J. W.; Ottewill, R. H.; Pelton, R.; Vianello, G.; Yates, D. E. *Br. Polym. J.* **1978**, *10*, 173−180.
(49) Goodwin, J. W.; Hearn, J.; Ho, C. C.; Ottewill, R. H. *Br. Polym. J.* **1973**, *5*, 347−362.
(50) Raman, N. K.; Anderson, M. T.; Brinker, C. J. *Chem. Mater.* **1996**, *8*, 1682−1701.

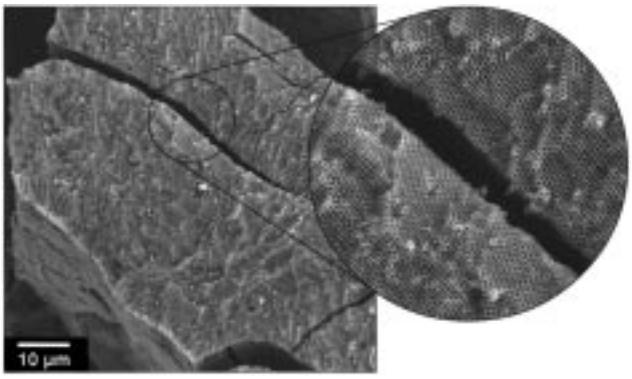

Figure 3. SEM of a macroporous TiO_2 crystal (anatase) with voids ordered over tens of micrometers (110 × 60 × 50 μm).

micrometers. Most particles observed in the SEM showed steps, facets, and edges (e.g., Figures 4a,d). Although many of these regions were defect-free, some areas showed point defects and, especially in large crystals, stacking faults, analogous to our observations for the latex sphere templates. In addition, large ordered domains were sometimes separated by cracks running through the pseudocrystal. Channels may have been created when the alkoxide was drawn through the bed of templating spheres by suction or during the subsequent template removal process.

The structure of the pseudocrystals was indexed by a series of tilting TEM experiments. Several ordered macroporous particles of silica, titania, zirconia, and zirconia/yttria were tilted through 90° tilt along one

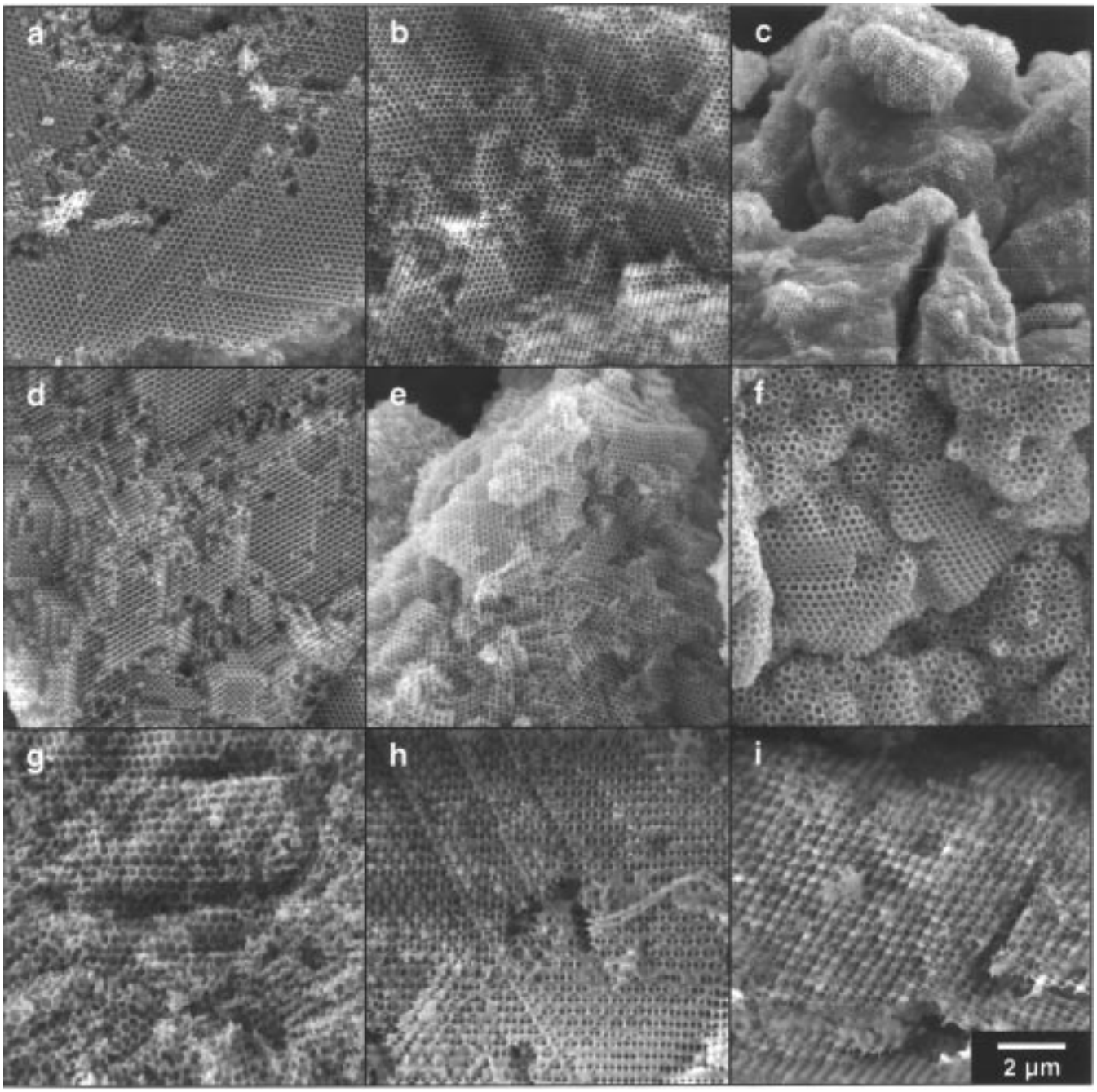

Figure 4. SEM images of macroporous titania, zirconia, and silica samples synthesized from alkoxides at various dilution levels. The fractions of alkoxide in solvent are (a) 100% TET, (b) 43% TET, (c) 14% TET, (d) 70% TPZ (30% *n*-PrOH, 0% EtOH), (e) 21% TPZ (9% *n*-PrOH, 70% EtOH), (f) 15% TPZ (6% *n*-PrOH, 79% EtOH), (g) 100% TEOS, (h) 70% TEOS, and (i) 55% TEOS.

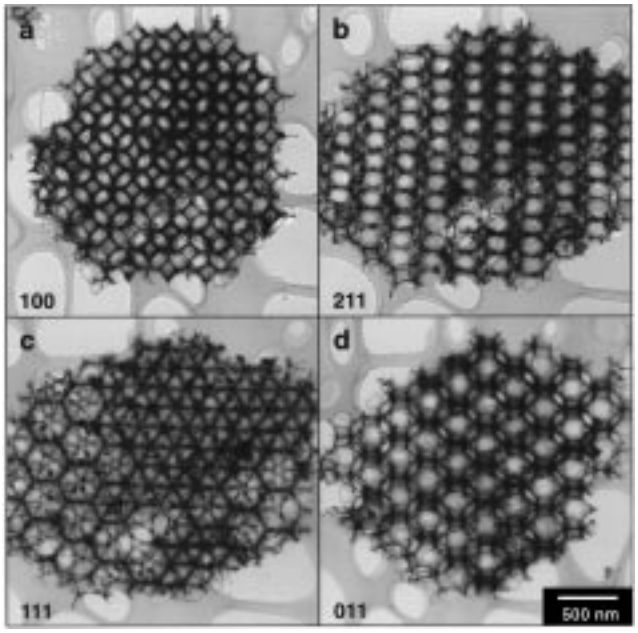

Figure 5. A series of four TEMs of an Y−Zr oxide sample tilted through 90° showing four different orientations. The directions were indexed to an fcc lattice by taking the Fourier transform of each image and comparing its spatial periodicity and tilt angle to a theoretical fcc lattice. (a) 0°, [100] direction, plane group p4mm; (b) 35.3°, [211] direction, plane group p2mm; (c) 54.7°, [111] direction, plane group p6mm; (d) 90°, [110] direction, plane group c2mm.

axis. When the pores were in alignment with the beam direction, the angle was noted and a picture was recorded. These images were analyzed by Fourier analysis to determine their spatial periodicity, and an example is shown in Figure 5. In each image, the dark areas correspond to the ceramic framework and the light areas to the void space. Background structure in the image is a result of the holey carbon support upon which the samples were loaded. The direct images and Fourier transforms (not shown) are consistent with views along [100], [211], [111], and [011] directions for a lattice formed by filling the interstitial spaces of an fcc array of spheres (space group $Fm\bar{3}m$, no. 225).

The wall thicknesses and sizes of window openings between walls depended on the alkoxide precursors, in particular the viscosity and hydrolysis or condensation rates of the precursors. Average wall thicknesses are listed in Table 2. These parameters could be controlled to some extent by diluting the precursors with alcohols and by adjusting the humidity of the environment. Addition of alcohols could modify the hydrolysis and gelation rates of the alkoxides. The order of void spaces was also affected by viscosity and dilution. Ordered structures were obtained only in a limited dilution range.

The effects of alkoxide dilution with alcohol were studied for macroporous silica, titania, and zirconia samples. The SEM images in Figure 4 depict the changes in wall thickness and ordering of the mesopores for products obtained at various dilution ratios. Figures 4a−c show examples for macroporous titania samples, obtained from TET with ethanol as diluent. The number of structural defects increased with increasing amounts of ethanol, and disordered macroporous structures were formed at TET/ethanol ratios below ≈21:79. At the same time the fraction of inorganic material in the composite product decreased, as shown in Table 1. The effects of diluting the zirconium alkoxide precursor with alcohol were similar to those observed for titania. Dilution in ethanol resulted in the formation of less ordered structures, as shown in the SEM images in Figures 4d−f. At higher dilution, the alcohol may have partially dispersed the colloidal latex crystal, causing the decrease in order observed for the templated oxides.

Figures 4g−i show that by adjusting the concentration of TEOS added to the latex spheres with ethanol, it was possible to control the wall thicknesses and window sizes between voids. The ability to vary the dimensions of the walls, as well those of the pores in a controlled fashion is important in certain applications, such as photonic crystals, so that the periodicity in the dielectric constant can be adjusted. The average wall thickness of the pure TEOS sample in Figure 4g was ≈90 nm. As ethanol was added to the TEOS synthesis mixture (TEOS/ethanol = 70:30 wt/wt), the openings

Table 2. Wall Compositions, Dimensions, Surface Areas, and Porosity Data for the Macroporous Solids

sample composition (preparation)[a]	phase (PDF file no.)[b]	surface area[c] (m^2/g)	pore volume[d] (mL/g)	median pore diameter[e] (nm)	wall thickness[f] (nm)	wall particle size[f] (nm)
SiO_2						
(100:0)	amorphous	173 [0.11]	0.38 [0.91]	8.9 [180]	58−132	N/A
(70:30)	amorphous	220 [0.55]	0.39 [1.39]	6.9 [190]	39−94	N/A
(55:45)	amorphous	231 [2.95]	0.44 [1.75]	7.3 [460]	33−74	N/A
(100:0, surfactant)	mesoporous walls	1337	0.80	2.3	29−37	N/A
TiO_2						
(extraction)	amorphous	157	0.36	21.1	37−58	N/A
(575 °C)	anatase (21−1272)	50 (22)	0.26	N/A	24−36	20−35
(1000 °C)	anatase/rutile	18	0.07	N/A	19−67	18−99
ZrO_2	baddeleyite (37−1484)	9 (38)	0.06	N/A	9−13	8−13
$Al_2O_3 \cdot xH_2O$	amorphous	195	0.63	10.5	4−6	N/A
Fe_2O_3	hematite (33−0664)				22−52	22−120
Sb_4O_6	senarmontite (43−1071)				12−66	12−156
WO_3	tungsten trioxide (43−1035)				14−32	8−68
$Y_{0.043}Zr_{0.957}O_2$	yttria-stabilized zirconia (30−1468)				8−41	6−29

[a] For silica, the ratios in parentheses refer to dilution values (TEOS/ethanol). For titania, the sphere removal method is listed. [b] Phases were identified by selected area ED and PXRD. [c] BET surface areas obtained with a Micromeritics ASAP 2000 V3.00 sorption analyzer, except for values in parentheses, which were obtained with an RXM-100 sorption analyzer. Values in square brackets are total pore areas obtained from mercury porosimetry at pressures between 0 and 2500 psia. [d] Average BJH pore volumes from the adsorption pore volume plots. Values in square brackets are intrusion volumes obtained from mercury porosimetry. [e] Average BJH pore diameters from the adsorption pore volume plots. Values in square brackets are median pore diameters obtained from mercury porosimetry. [f] Wall thicknesses and particle sizes were estimated from TEM images (N/A = not applicable).

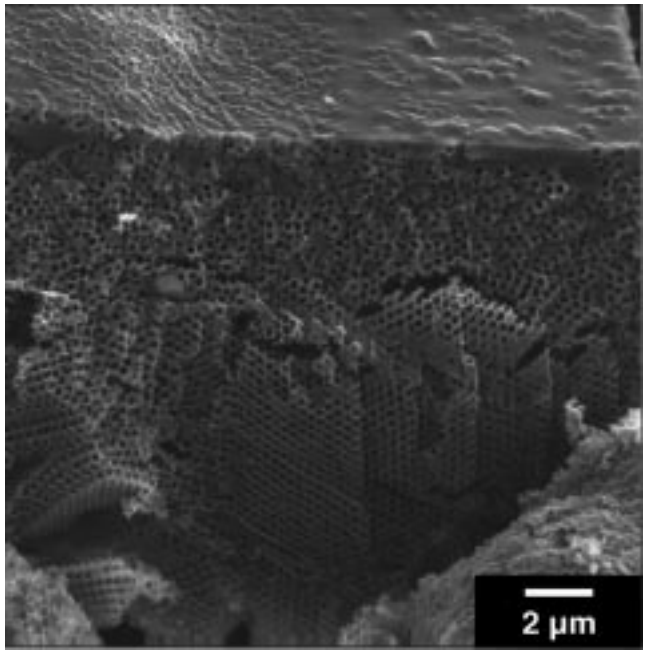

Figure 6. SEM of a macroporous anatase particle showing gradients in the density of the inorganic component and gradients in the order of voids.

between pores increased considerably and the average wall thickness decreased to ≈67.5 nm (Figure 4h). In this figure, it was possible to observe the macropore openings (darker holes) in the layer underneath the first layer. For a TEOS/ethanol weight ratio of 55:45, the SEM micrograph (Figure 4i) depicts a highly ordered macroporous structure with even larger windows and an average wall thickness of ≈54 nm. This micrograph shows a high degree of interconnectivity between voids and 3D periodicity in multiple layers. Mercury porosimetry (limited to 2500 psia) revealed a small increase in intrusion volume, total pore area, and median pore diameter, as TEOS was diluted (Table 2). An SEM of the sample obtained from a 55:45 TEOS/ethanol solution confirmed that the framework remained intact at this pressure, which falls within the pressure ranges utilized in high-pressure liquid chromatography. The framework fractured after a porosimetry measurement carried out at pressures up to 31 000 psia.

Some of the possible effects of sample preparation technique are evident in Figure 6, which shows the SEM of a calcined titania sample exhibiting three different regions: a dense phase, monodisperse disordered macropores, and ordered macropores from top to bottom. The dense phase arose from the use of excess alkoxide in the synthesis. The extra reagent did not percolate through the spheres and formed a thick crust on the top. Only a few pores were present in the solid phase as a consequence of some latex spheres escaping. Other spheres could not escape, resulting in small amounts of residual carbon in the bulk analysis of such samples. The disordered, intermediate phase was probably the result of surface agitation and the inability of the spheres to coalesce again upon drying. Similar disorder was observed in samples prepared from highly diluted Ti or Zr alkoxides. The bottom of the SEM micrograph in Figure 6 displays order over a length of ≈15 μm and illustrates the penetration depth of the inorganic precursor through multiple layers of spheres.

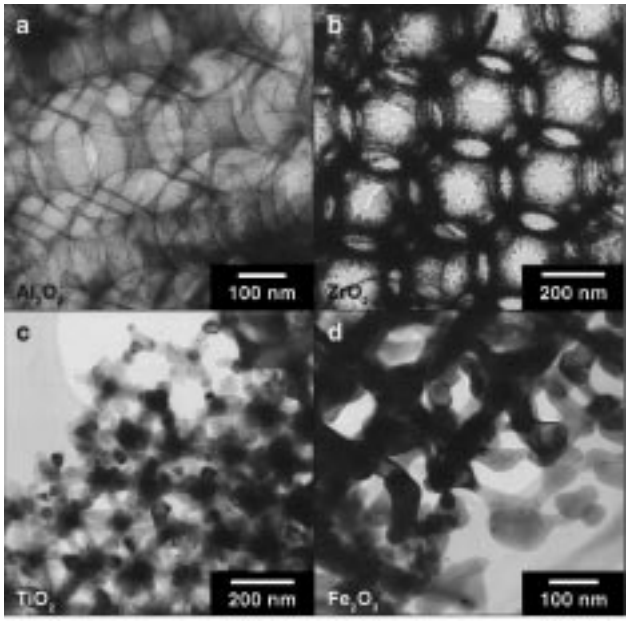

Figure 7. (a) TEM showing the gossamer "sheet" structure of the walls of a macroporous alumina particle a few degrees from its [100] orientation. (b) Bright field TEM image of macroporous zirconia in the [011] orientation. Small crystalline appendages are visible along the edges of the dark "rods." (c) TEM of macroporous titania prepared by calcination at 1000 °C for 2 h, showing crystals that are considerably larger than in a sample calcined at 575 °C for 8 h. (d) TEM of the wall structure of macroporous iron oxide oriented along [100].

Wall Structure. The wall structure of the macroporous solids can be classified into three categories: sheets, rods, and large crystals. Figure 7 shows TEM images of each category. Figure 7a provides a good example of a "sheet" wall structure. The walls of this macroporous alumina sample were extremely thin (≈4−6 nm) and amorphous. Nodes in the skeleton were occupied by a filled diamond (sometimes nearly square) when viewed along the [100] orientation. In many other samples, the diamond was not filled, resulting in a lower surface energy (see, for example, Figure 5a). A "rod" structure was exhibited by macroporous zirconia, where rods converged in nodal points (Figure 7b). The walls were in fact polycrystalline, but the crystals were smaller than the average wall thickness. Walls consisting of larger crystallites (anatase) were formed, for example, in macroporous titania prepared by calcination at 1000 °C for 2 h (Figure 7c). Similar large crystallites of hematite were visible in the sample of macroporous iron oxide (Figure 7d). For the samples investigated thus far, an increase in wall particle size led to a reduction in periodicity of the macropores.

The walls of the macroporous sieves were identified as amorphous or crystalline phases based on PXRD measurements of the bulk materials and on selected area ED patterns obtained by TEM. Amorphous walls exhibited additional mesoporosity leading to higher surface areas. The observed phases and dimensions of the walls are listed in Table 2 and are discussed later in more detail for each composition. As expected, the oxides formed walls composed of the thermodynamically most stable phase at a given processing temperature.

Macroporous Silica. The walls in macroporous silica samples were X-ray amorphous. They were further

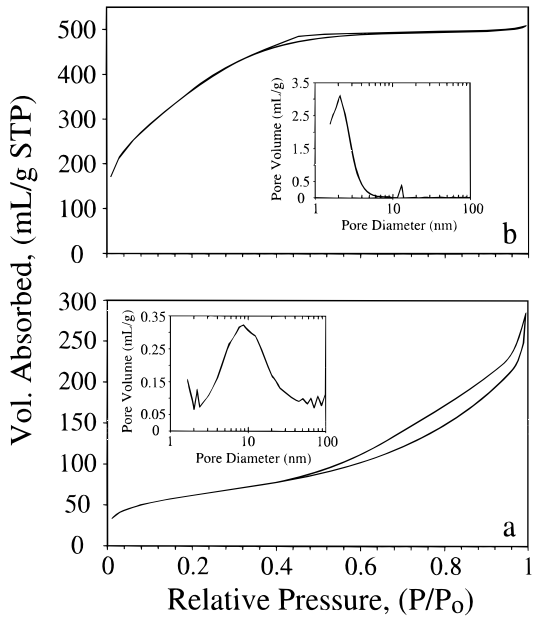

Figure 8. Nitrogen adsorption isotherms and pore size distribution plots for macroporous silica. (a) Undiluted TEOS was used as precursor. No surfactant was added during the synthesis. (b) Surfactant added.

characterized by nitrogen adsorption measurements and solid-state ^{29}Si MAS NMR spectroscopy. Table 2 lists the nitrogen adsorption results obtained for materials prepared from pure TEOS, and from the TEOS/ethanol systems already mentioned. A Type II nitrogen adsorption isotherm with some adsorption hysteresis was observed for all three silica materials (Figure 8a). The shape of the isotherm, in particular the large rise in adsorption at increased relative pressures, was characteristic for walls composed of tenuously assembled silica clusters.[51] Both BET surface areas and BJH pore volumes increased upon dilution of TEOS with ethanol. The adsorption pore volume plots for the three silica materials showed a broad distribution of mesopores with diameters of ≈2−40 nm, indicative of the glassy nature of the framework. These mesopores gave rise to surface areas between 173 and 231 m^2/g. The ^{29}Si MAS NMR spectra exhibited one broad resonance centered around −110 ppm, a value typical of Q^4 silicon atoms in silica glass.[52] The broad peak arises from a distribution of bond angles in the Q^4 tetrahedral units.

It was possible to create narrower mesopore distributions by combining a modified MCM-41 synthesis with the latex sphere templating process. A TEOS/surfactant mixture was percolated through a latex sphere array, followed by hydrolysis and condensation of the silicate precursor. After removal of both surfactant and polystyrene by calcination, the macroporous product closely resembled that shown in Figure 4g. The PXRD pattern showed a single, broad diffraction line at d = 2.8 nm, typical for mesoporous silicates with a weak degree of order. The Type I nitrogen adsorption/desorption isotherm (Figure 8b) showed a slow rise in the amount of nitrogen adsorption with increasing relative pressure and then approached a limiting value. It exhibited less hysteresis than the isotherms for the products of the surfactant-free syntheses, which has been interpreted to mean that the pores are smooth and cylindrical.[50] The surface area and pore volume of this sample were greatly increased (1337 m^2/g and 0.80 cm^3/g, respectively). The mesopore size distribution tightened significantly, with most mesopores being <4 nm with a peak at ≈2.3 nm. Thus, a combined meso-/macroporous structure was created by the dual-templating process. A similarly formed structure with a bimodal distribution of pore sizes has recently been reported by Antonietti et al.[25]

Macroporous Titania. The phase of the titania walls could be controlled by the conditions of template removal (see Table 2). An amorphous titania phase was obtained when the sample had undergone relatively mild heat treatments during Soxhlet extraction of polystyrene by a THF/acetone solution at temperatures <56 °C. Template removal by calcination at 450−575 °C resulted in the formation of anatase walls, and higher heat treatment (at 1000 °C) produced a macroporous sample containing mostly anatase and some bulk rutile. When a macroporous anatase sample was cooled and reheated to 1000 °C, rutile was formed, but the periodic void structure was lost by sintering. In related studies, rutile walls were created at 1000 °C in a synthesis of macroporous titania based on oil/formamide emulsions.[26] The nitrogen adsorption measurements for the titania phases are listed in Table 2. All three phases exhibited similar Type II isotherms with a small amount of high-pressure hysteresis. The isotherms are typical for unrestricted monolayer−multilayer adsorption on nonporous or macroporous adsorbents.[53] The surface areas and pore volumes decreased from amorphous titania to anatase prepared at progressively higher calcination temperatures, as small crystallites composing the walls continued to sinter and grow.

Macroporous Zirconia. The walls of macroporous zirconia after template removal by calcination at 575 °C for 7 h in air consisted of the crystalline baddeleyite phase. Figure 7b shows a TEM image of the baddeleyite microcrystals that were fused together to create a network. Type II nitrogen adsorption isotherms were obtained, similar to those observed for the titania samples. The measured BET surface areas of these materials were mostly due to the small particle size of the crystallites.

Macroporous Yttria-Stabilized Zirconia. The Y precursor for these samples, yttrium isopropoxide, was a solid and exhibited only limited solubility in zirconium *n*-propoxide. Nonetheless, with an Y/Zr ratio of 1/22 in the starting material, a remarkably ordered macroporous product was obtained. TEM combined with EDS showed that the Y was distributed evenly throughout the sample with an Y/Zr mole ratio of 1:32. The selected area ED pattern of the sample walls matched exactly with the powder diffraction file (PDF) pattern of cubic yttria-stabilized zirconia (PDF 30−1468).[54] The TEM images of the macroporous product viewed from differ-

(51) Brinker, C. J.; Scherer, G. W. *Sol−Gel Science: The Physics and Chemistry of Sol−Gel Processing*; Academic Press: San Diego, 1990.

(52) Engelhardt, G.; Michel, D. *High-Resolution Solid-State NMR of Silicates and Zeolites*; Wiley: Norwich, 1987.

(53) Gregg, S. J.; Sing, K. S. W. *Adsorption, Surface Area and Porosity*; Academic Press: London, 1967.

(54) McClune, W. F. *JCPDS − Powder Diffraction File*; International Center for Diffraction Data: Newton Square, PA.

ent tilting angles were already discussed (Figure 5). These images showed that the walls had a thickness and particle size comparable to the walls of pure macroporous zirconia. The particle sizes in the zirconia/yttria system ranged from 6 to 29 nm, with wall thicknesses between 8 and 41 nm. The high chemical resistance and low thermal expansion coefficient of yttria-stabilized zirconia make this material an attractive ceramic support.

Macroporous Alumina. During the synthesis of macroporous alumina in air, hydrolysis and condensation of aluminum tri-*sec*-butoxide occurred so quickly that dilution with 2-butanol was necessary. Even with 50 wt % dilution, small particulates formed almost immediately. Nonetheless, an ordered macroporous product was obtained upon removal of the latex spheres by calcination at 575 °C in air for 7 h. The walls of this material were thin amorphous sheets, exhibiting a high surface area (317 m^2/g). Nitrogen adsorption measurements of the calcined alumina sample gave a Type II isotherm with some hysteresis similar to that observed for the silica samples. The adsorption pore volume plot showed a very broad distribution in pore diameters from ≈2−100 nm. The majority of pores in the alumina sample arose from smaller mesopores with an average diameter around 10.5 nm. The ^{27}Al MAS NMR spectra revealed both octahedrally and tetrahedrally coordinated aluminum resonances at 12.0 and 41.9 ppm, respectively, with an intensity ratio of ≈4:1 for $Al_{Oh}Al_{Td}$.

Macroporous Antimony Oxide. Antimony(III) *n*-butoxide behaved in a fashion similar to zirconium *n*-propoxide and TET, except that upon calcination of the composite with latex spheres at 450 °C, the off-white macroporous product was less ordered than the samples already discussed. The walls were composed of senarmontite microcrystals (Sb_4O_6, PDF 43−1071). Cubic senarmontite is the thermodynamically stable form of antimony oxide below 570 °C and contains discrete Sb_4O_6 molecules.[55] At 570 °C, antimony oxide undergoes a phase transition to orthorhombic valentinite, in which alternate antimony and oxygen atoms are linked into bands, creating a macromolecular structure.[55,56] When an antimony oxide/latex sphere composite was calcined at 575 °C, nonporous, needlelike crystals were formed. As in the case of the anatase-to-rutile phase transition for macroporous titania, the latex-free macropore structure could not withstand the internal stresses during the cubic-to-orthorhombic phase transition of antimony oxide, which resulted in the loss of the macropore structure.

Oxides of Iron, Tungsten, and Vanadium. These transition metals can exhibit multiple oxidations states. The synthesis of macroporous iron oxide was different from the preparation of most other samples because the starting material, iron(III) ethoxide was a brown-black solid rather than a liquid. A 25 wt % solution in ethanol was able to penetrate the latex spheres. After calcination for 6 h in air at 450 °C, it produced many areas of rust-colored, ordered macroporous Fe_2O_3, although some nonporous bulk material existed in the sample. The walls in the macroporous sample were composed of ≈22−120-nm-sized hematite microcrystals (Figure 7d). The dimensions of individual particles were sometimes larger than the average wall thicknesses listed in Table 2 because some particles were elongated and orientated with the largest dimension along the wall direction. Longer heating times and higher temperatures created a porous, disordered material. Tungsten(V) ethoxide was less viscous and less reactive than either TET or zirconium *n*-propoxide. After calcination of the latex sphere composite at 450 °C, the product was a bright yellow-green macroporous tungsten(VI) oxide (WO_3, PDF 43−1035). Like the macroporous iron oxide, the structure was partially ordered but less periodic than the samples already discussed. Calcination at 575 °C created a porous, disordered material. Upon reduction under flowing hydrogen at 400 °C for 8 h, the powder became blue, which is indicative of the formation of a nonstoichiometric oxide, WO_x ($2 < x < 3$). Vanadium oxide did not form the "honeycomb" structure under the conditions listed in the *Experimental Section*. Instead, latex-templated vanadium oxide, heated to 450 °C, produced nonporous red-orange elongated crystals that were a few micrometers in length. Macroporous vanadium oxide could be obtained when the polystyrene templates were removed at lower temperatures (between 250 and 300 °C, 12 h); however, these products were not highly ordered and dense bulk vanadium oxide was present as a side product.

Macroporous Aluminophosphates. The walls in the ordered macroporous aluminophosphate obtained after calcination were X-ray amorphous and had an Al/P ratio of 1.7. The ^{27}Al MAS NMR spectrum of this sample showed resonances for tetrahedral Al at 41.0 ppm and for octahedral Al at −14.5 ppm, with an intensity ratio of ≈6:1. The ^{31}P MAS NMR spectrum exhibited a single sharp resonance at −26.1 ppm, which is typical for $P(OAl)_4$ environments in $AlPO_4$ materials. Both the ^{27}Al and the ^{31}P NMR shifts data indicated that the tetrahedral Al was surrounded by four tetrahedral phosphate groups, forming the aluminophosphate framework. The absence of a ^{31}P resonance at higher frequency (e.g., −14 ppm) suggested that phosphorus was not bonded to octahedral Al and that the octahedral Al was present as extraframework Al. A BET surface area of 17 m^2/g and a relatively low pore volume of 0.04 mL/g indicated that the aluminophosphate walls did not exhibit any micro- or mesoporosity.

Hybrid Organic/Inorganic Macroporous Solids. Mesoporous silicates, related to MCM-41, with organic surface functional groups have recently been synthesized in a direct "one pot" synthesis.[16−18,57] They were formed using organotrialkoxysilane precursors diluted with tetraalkoxysilanes. In the case of studies involving vinyl, thiol, and sulfonic acid groups, it was shown that the organic groups were incorporated in the condensed framework, most of them were present in the mesopore channels, and that they were accessible for further functionalization. Similar mixtures incorporating Si−C bonds in a silicate network could be formed using the latex sphere templating technique. The polystyrene

(55) Smith, J. D. *Comprehensive Inorganic Chemistry*; Bailar Jr., J. C., Emeléus, H. J., Sir Nyholm, R., Trotman-Dickenson, A. F., Eds.; Pergamon Press: Oxford, 1973; Vol. 2, pp 547−683.

(56) Roberts, E. J.; Fenwick, F. *J. Am. Chem. Soc.* **1928**, *50*, 2125−2147.

(57) Huo, Q.; Margolese, D. I.; Stucky, G. D. *Chem. Mater.* **1996**, *8*, 1147−1160.

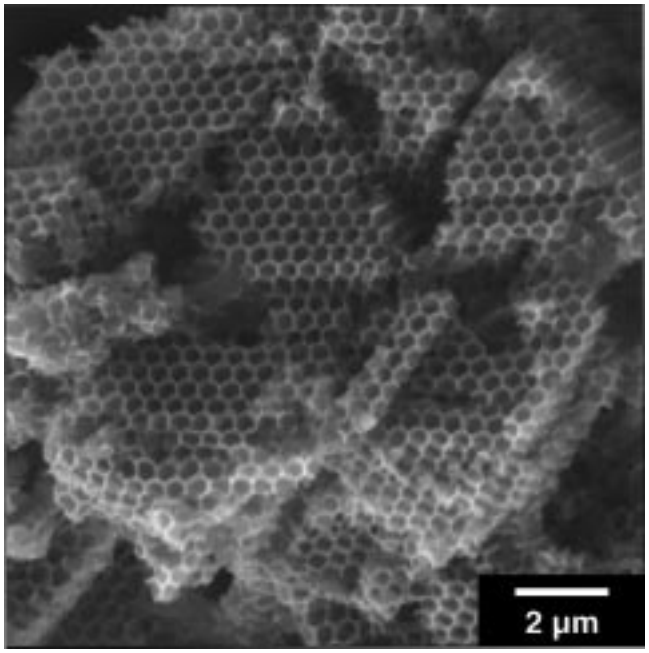

Figure 9. SEM image of hybrid macroporous silica with vinyl functional groups synthesized from 5 TEOS:1 VTES precursors. The latex spheres were removed by extraction.

could be selectively removed by extraction from the macroporous silicates that were functionalized with vinyl or 2-cyanoethyl groups, leaving a large fraction of functional groups intact. For both compositions, the macropores were well ordered, although particle sizes were typically smaller than for the pure oxides (a few μm, Figure 9). Periodic structures were obtained with VTES/TEOS mole ratios as high as 1:1.8. The FT-IR spectra of the vinyl-modified macroporous silicates showed a peak at 1636 cm^{-1} corresponding to the C═C stretching vibration of the vinyl group, an absorption at 1412 cm^{-1} assigned to the vinyl CH_2 in-plane deformation, an absorption at 975 cm^{-1} for the CH out-of-plane deformation, and a peak at 1279 cm^{-1} corresponding to the Si−C stretch. The cyanoethyl-modified silicate exhibited a C≡N stretching vibration at 2255 cm^{-1}. An additional peak at 1731 cm^{-1} suggested that some conversion to a carboxylic ester occurred during the synthesis of this sample.

Efficiency of the Synthesis. Although scale-up should be possible, the present synthesis scale has been limited to tens of milligrams of ordered, template-free product and to macroporous crystal sizes mostly below one millimeter along each dimension. Several factors contributed to the small mass of product obtained at this stage. One was the intrinsic low density of these highly porous materials. Other factors were related to the present synthetic procedure. Although yields based on alkoxide imbibed in the colloidal latex crystals were reasonable (see section on *Removal of Latex Spheres*), some extraneous alkoxide often passed through the template array. For example, in case of the titania synthesis, only 5−16 wt % of alkoxide adhered to the latex spheres, and 12−23 wt % for zirconia. The amount adhering to the surface was a function of alkoxide dilution in alcohol. For titania and zirconia, an optimal range was found between 40 and 60 wt % alkoxide in alcohol. To make the synthesis economically more feasible, the unreacted alkoxide could be recycled in another synthesis. In terms of polystyrene spheres used, yields were typically 40−160 mg of calcined titania or zirconia product per gram of latex spheres. When the spheres were extracted, the polystyrene could be recycled for different applications, but the spherical shapes of the polymer were lost. We are presently investigating a number of options for scale-up and for more efficient syntheses, including syntheses under inert atmospheres and packing of ordered templates in columns, as well as thin films.

Conclusions

The method of synthesis of ordered macroporous products appears to be quite general and applicable to many wall compositions. It is simple and based on readily available precursors. Although various void packing arrangements are possible, a diamond-like lattice was identified for the framework of several samples. Some control exists over the wall thickness and porosity. Control over the wall thickness would be important, for example in adjusting the optical properties of photonic crystals, an application which has already been demonstrated for macroporous titania.[30] Ordered structures with multiple wall phases (e.g., amorphous or crystalline) could be achieved with certain compositions. However, phase transformations that occurred upon heating the sample after the latex sphere templates had been removed tended to result in the loss of an ordered or even a porous structure. The most ordered structures were obtained with oxide compositions that could be calcined well below a phase transition temperature (titania, zirconia, or yttria-stabilized zirconia) or with materials that formed amorphous wall phases (especially silica).

Many interesting properties are foreseen for the macroporous solids studied here, including physical (optical, mechanical) and chemical properties (reactivity, catalytic activity). These properties will be investigated for each composition in more detail in the future. Various applications could potentially profit from these materials. For example, catalysis and large-molecule separation processes could benefit from more uniform porous supports that provide optimal flow and improved efficiencies. The pores are in a size regime that permits immobilization and stabilization of large guest molecules, including biological molecules. Because walls could be composed of semiconducting as well as insulating materials, applications as porous electrodes or electrolytes may be possible.

Acknowledgment. We acknowledge 3M, Dupont, the David and Lucille Packard Foundation, the McKnight Foundation, and the National Science Foundation (DMR-9701507) for support of this research. We thank Professor W. G. Miller and Mr. D. G. Gold for assistance with the latex sphere preparation, and Victor Young for helpful discussions. B. T. H. and C. F. B. thank the Center for Interfacial Engineering at the U of M for a CIE-NSF graduate fellowship.

CM980666G